



## Research paper

# Experimental study on dynamic stability of rubber-cement composites by SHPB and high-speed slicing

Rongzhou Yang<sup>1</sup>, Ying Xu<sup>2,3</sup>, Pei Yuan Chen<sup>3</sup>

**Abstract:** Improper disposal of waste tires will not only bring environmental impact and safety risks but also cause a serious waste of resources. In the field of civil engineering materials, waste tire particles are used as a substitute for non-renewable aggregates to produce flexible rubber-cement composites (RCC). To explore the high-speed slicing stability of RCC, this test took normal cement mortar (NCM) and rubber cement mortar (RCM) as research objects. The SHPB tests with the same impact energy level and the high-speed slicing tests with a slice thickness range of about 1.4 mm ~ 4.4 mm were carried out. The results showed that NCM and RCM showed different stability differences in the process of high-speed slicing. In the case of ensuring the integrity of the slice, the minimum thickness of the slice can be better decreased with the increase of the rubber content. Finally, from the perspectives of split Hopkinson pressure bar (SHPB) test results and mesoscopic structure states, the essential reason for ensuring the stability of high-speed slicing lied in the improvement of rubber particles (dominant role) and pores on material deformation and flexible energy dissipation.

**Keywords:** rubber-cement composites, split Hopkinson pressure bar (SHPB), high-speed slicing, deformation and fracture, slice thickness

<sup>1</sup>PhD., State Key Laboratory of Mining Response and Disaster Prevention and Control in Deep Coal Mines, School of Civil Engineering and Architecture, Anhui University of Science and Technology, Huainan 232001, China, e-mail: [rongzhouy@outlook.com](mailto:rongzhouy@outlook.com), ORCID: 0000-0002-0126-2446

<sup>2</sup>Prof., State Key Laboratory of Mining Response and Disaster Prevention and Control in Deep Coal Mines, School of Civil Engineering and Architecture, Anhui University of Science and Technology, Huainan 232001, China, e-mail: [yxu@aust.edu.cn](mailto:yxu@aust.edu.cn), ORCID: 0000-0001-8438-3130

<sup>3</sup>Assoc. Prof., School of Civil Engineering and Architecture, Anhui University of Science and Technology, Huainan 232001, China, e-mail: [yxu@aust.edu.cn](mailto:yxu@aust.edu.cn), ORCID: 0000-0002-5538-617X

## 1. Introduction

Concrete composites are used in many types of infrastructure and protective engineering [1–3]. Protecting infrastructure is essential for economic development and improving the quality of life [1]. However, the poor performance of concrete in ductility, fatigue resistance, impact resistance, and seismic resistance has aroused people's concern about its performance [3].

More importantly, with the further development and construction of deep underground resources and engineering facilities, in a series of disaster prevention and reduction problems, such as supporting the stability of surrounding rock of roadway/tunnel [4], seismic stability of the spatial structure [5], protection of vehicle high-speed impact [6], and protection of explosion impact [7]. It has become the consensus of researchers to use civil engineering materials with cost-effectiveness, high-deformation, and cushioning energy dissipation to solve the above problems [4–7]. Therefore, in recent years, people pay more and more attention to the development of flexible concrete and its mechanical properties test.

“The four major environmental concerns related to the accumulation of waste tyres are tyre fires, leachates, breeding grounds for pest species, and land use (black pollution)” [8]. At the same time, the rapid development of the construction industry has consumed huge natural resources, resulting in a continuous decline in natural resources, which has also accelerated the research work to promote the use of recyclable waste tyres, especially in the field of civil engineering materials, waste tire particles are used as a substitute for non-renewable aggregates (natural aggregates) [8,9]. The above alternative makes RCC with better flexible deformation and energy dissipation performances has attracted the attention of researchers in fatigue resistance [10], impact resistance [11], explosion resistance [12], seismic resistance [13], and researchers have carried out more experimental research on them.

But so far, the high-speed slicing test of RCC has not been considered by researchers. Combined with the SHPB impact test, the high-speed slicing stability (Stability refers to the impact resistance and crack resistance of RCC under dynamic disturbance) of RCC was discussed to effectively solve the problem of “black pollution” and promote the application of RCC in disaster prevention and support engineering. This work took NCM and RCM as research objects, and the SHPB impact tests and the high-speed slicing tests with slice thickness ranging from about 1.4 mm to 4.4 mm were carried out. The innovation points are as follows: 1) High-speed slicing test of RCC was carried out for the first time, making up the blank of high-speed slicing test research of RCC. 2) The relationship between the thickness, integrity, and stability of RCM high-speed slicing and the content of rubber was discussed, and the stability mechanism of RCC under high-speed slicing was discussed and analysed from the point of view of impact deformation, energy dissipation, and mesoscopic structures.

## 2. General situation of test

### 2.1. Materials and mix proportions

Table 1 shows the parameters of materials. The grain size grading curves of the river sand and rubber particles used in the test are shown in Fig. 1. RCM was prepared by

replacing natural river sand with an equal volume of rubber particles in the experiment. According to the standard JGJ/T 98-2010 [14], the mix proportions ( $W/C = 0.5$ ) are listed in Table 2.

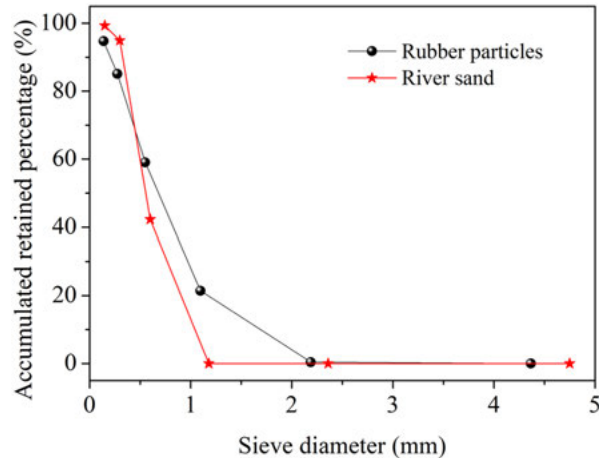


Fig. 1. The grain size grading curves of the river sand and rubber particles

Table 1. Physical parameters of materials

Parameter	Cement	Parameter	River sand	Parameter	Rubber particles
Type specification	P · O 42.5	Density ( $\text{kg/m}^3$ )	2680	Surface geometry	Irregular polyhedron
Compressive strength (MPa) – 28 days	> 42.5	Fineness modulus	2.36	Density ( $\text{kg/m}^3$ )	1150
CaO (wt.%)	61.9	Particle size (mm)	$\leq 1.18$	Mesh	20
SiO <sub>2</sub> (wt.%)	20.9	Passing (%) Sieve size 2.36 mm	100%	Rubber hydrocarbon (%)	42

## 2.2. Fabrication process

The fabrication process mainly included three aspects: fresh mortar mixing (According to the standard JGJ/T 70-2009 [15], the stirring time should not be less than 120 s), pouring molding of the cylindrical specimen ( $\varnothing 70$  mm), and standard curing (Curing for 28 days in a standard curing environment with a humidity > 90% and temperature =  $20 \pm 2^\circ$ ) [15]. The specific fabrication process is shown in Fig. 2.

Table 2. Mix proportion design (Mass ratio)

Sample type*	Water	Cement	River sand	Rubber particles
NCM-0	1	2	4	0
RCM-20	1	2	3.2	0.343
RCM-40	1	2	2.4	0.686
RCM-60	1	2	1.6	1.030
RCM-80	1	2	0.8	1.373

\*Note: The values in the sample types are rubber content.

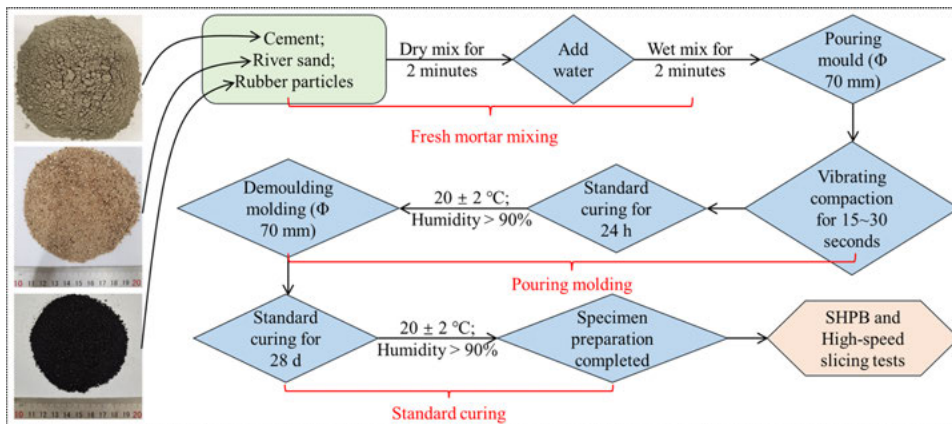


Fig. 2. Schematic diagram of specific fabrication process

## 2.3. Test methods

To better explore the dynamic stability of rubber-cement composites, this work includes two different dynamic testing methods: SHPB impact compression and high-speed slicing. The specific test contents are as follows:

### 1. SHPB test

With the help of a variable cross-section SHPB loading system, the impact compression tests of NCM and RCM specimens with a size of  $\varnothing 70$  mm  $\times$  35 mm were carried out at the same impact energy level (about 138 J). The schematic diagram of the SHPB loading system used in the test is shown in Fig. 3, and the relevant parameters of the compression bars are shown in Table 3.

Table 3. Parameters of bar components and strain gauges [16]

Parameter	Incident & transmitted bars	Parameter	Resistance strain gauge	Semiconductor strain gauge
Diameter (mm)	74	Resistance value ( $\Omega$ )	$120 \pm 1$	120
Wave velocity (m/s)	5190			
Young's modulus (GPa)	210	Sensitivity coefficient	$2 \pm 0.01$	$110 \pm 0.05$
Density ( $\text{g/cm}^3$ )	7.8			

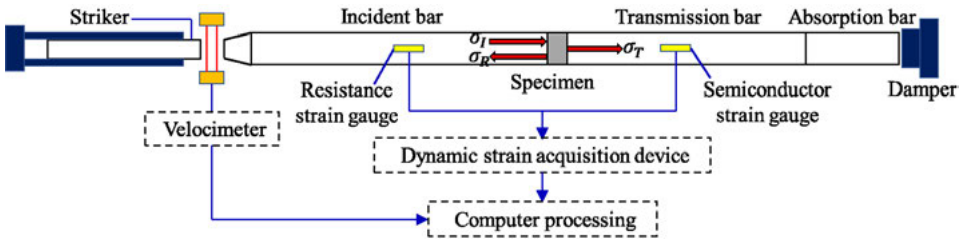


Fig. 3. SHPB loading system

The strain rate ( $\dot{\varepsilon}$ ), strain ( $\varepsilon$ ), and stress ( $\sigma$ ) of the specimen under SHPB dynamic compression can be calculated by the simplified three-wave method Eq. (2.1) [17].

$$(2.1) \quad \begin{cases} \dot{\varepsilon}(t) = \frac{C}{L_S} [\varepsilon_I(t) - \varepsilon_R(t) - \varepsilon_T(t)] \\ \varepsilon(t) = \frac{C}{L_S} \int_0^t [\varepsilon_I(t) - \varepsilon_R(t) - \varepsilon_T(t)] dt \\ \sigma(t) = \frac{A}{A_S} E \varepsilon_T(t) \end{cases}$$

where:  $E$  – elastic modulus of compression bar (GPa),  $A$  – cross-sectional area of compression bar ( $\text{m}^2$ ),  $C$  – wave velocity of compression bar,  $A_S$  – initial cross-sectional area of the specimen ( $\text{m}^2$ ),  $L_S$  – initial length of the specimen (m),  $\varepsilon_I$  – incident strain in compression bar,  $\varepsilon_R$  – reflected strain in compression bar,  $\varepsilon_T$  – transmitted strain in compression bar.

The incident energy ( $W_I$ ), reflection energy ( $W_R$ ), transmission energy ( $W_T$ ), and damage energy ( $W_D$ ) of the specimen under SHPB dynamic compression can be calculated

by Eq. (2.2) [17].

$$(2.2) \quad \left\{ \begin{array}{l} W_I(t) = AEC \int_0^t \varepsilon_I^2(t) dt \\ W_R(t) = AEC \int_0^t \varepsilon_R^2(t) dt \\ W_T(t) = AEC \int_0^t \varepsilon_T^2(t) dt \\ W_D(t) = W_I(t) - W_R(t) - W_T(t) \end{array} \right.$$

## 2. High-speed slicing test

The thin slice cutting tests of cylindrical specimens NCM and RCM were carried out by using a high-speed cutting machine with a rotational speed of 2890 r/min and a blade thickness of about 3.15 mm. The details are as follows: 1) According to the rubber content, the specimens were divided into five groups, each group of three parallel specimens. 2) The slice thickness was kept between about 1.4 mm and 4.4 mm. 3) The states of the specimens in the process of slicing were recorded by photography and video.

## 3. Test results and discussion

### 3.1. SHPB test

#### 1. Typical three-wave graph

Typical three-wave graphs of the specimens under the SHPB impact compression tests are shown in Fig. 4. It can be seen from Fig. 4 that the incident wave curves basically coincide, which effectively ensured that the test was carried out at the same level of incident

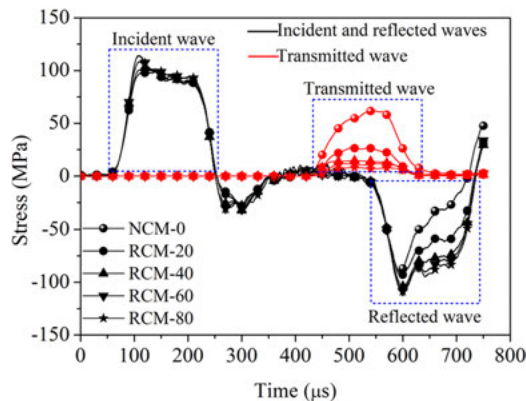


Fig. 4. Typical three-wave graphs of specimens under SHPB tests

energy (impact energy). It can be found that with the increase of rubber content, the peak values of the reflected waves and transmitted waves increased and decreased respectively, which showed that the addition of rubber played a serious role in hindering the propagation of stress waves [16, 17].

## 2. Stress-strain curve and dynamic strength

The stress-strain curves and dynamic strength of the specimens under the SHPB impact compression tests are shown in Fig. 5. As can be seen from Fig. 5a, compared with the NCM, the stress-strain curves of RCM showed an obvious yield platform. The length of the yield platform ( $\Delta\varepsilon$ ) increased significantly with the increase of rubber content (the maximum increase is 89.35%), which indicated that RCM had excellent ductile deformation characteristics. As can be seen from Fig. 5b, the dynamic strength of the specimens decreased significantly with the increase of rubber content (the maximum decrease is 87.53%), and the attenuation rate of dynamic strength decreased with the increase of rubber content.

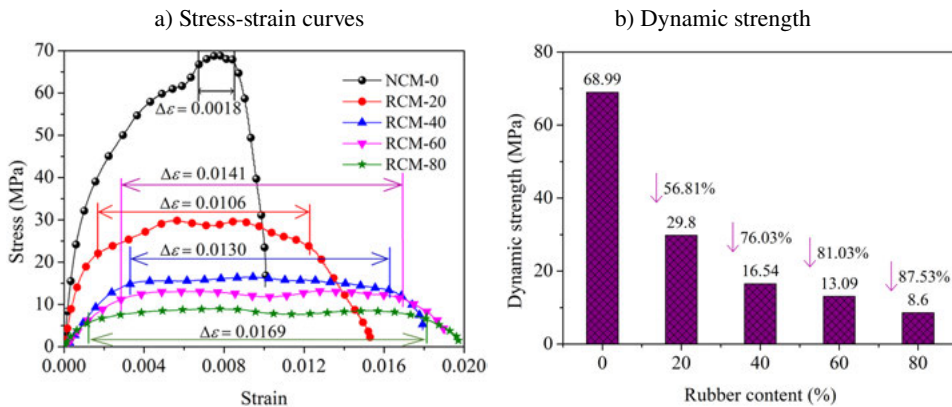


Fig. 5. Stress-strain curves and dynamic strength of specimens under SHPB tests

## 3. Strain-time curve and ultimate strain

The strain-time curves and ultimate strain of the specimens under the SHPB impact compression tests are shown in Fig. 6. As can be seen from Fig. 6a, the strain-time curves can be divided into three evolution stages: non-strain damage (*OA*), strain damage (*AB*), and strain stability (*BC*). The specific manifestations are as follows:

1. *OA* stage (0 ~ 60  $\mu\text{s}$ ): at this stage, the specimens mainly occurred initial compaction deformation and elastic-plastic deformation, which belonged to the pre-peak deformation stage, so there was basically no strain damage at this stage (strain damage is the damage caused by excessive strain).
2. *AB* stage (60 ~ 180  $\mu\text{s}$ ): at this stage, the specimens mainly occurred yield-plastic deformation, and the specimens produced strain damage due to excessive plastic strain.

3. *BC* stage (180 ~ 210  $\mu$ s): at this stage, the specimens mainly occurred fracture-plastic deformation, the strain tended to be stable, and the strain damage of the specimen reached the maximum.

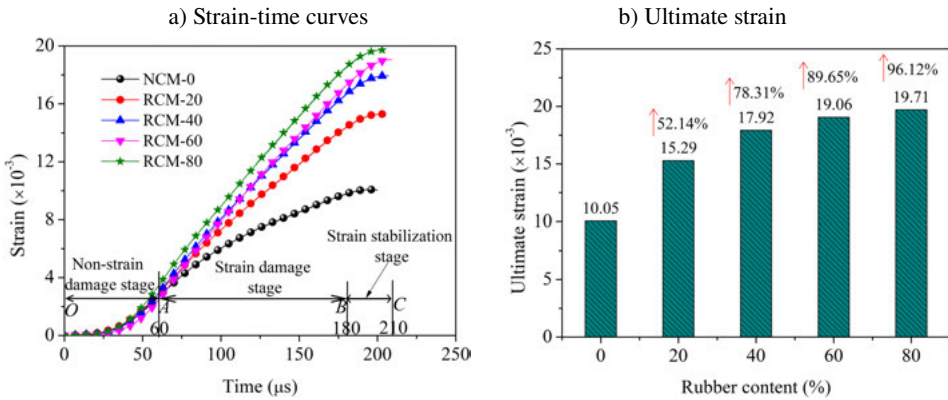


Fig. 6. Strain-time curves and ultimate strain of specimens under SHPB tests

It can be seen from Fig. 6b that the ultimate strain of the specimens increased with the increase of rubber content (the maximum increase is 96.12%), which showed that RCM had excellent deformability.

#### 4. Strain rate-time curve and average strain rate

The strain rate-time curves and average strain rates of the specimens under the SHPB impact compression tests are shown in Fig. 7. As can be seen from Fig. 7a, the strain rate-time curves can be divided into three evolution stages: rapid growth (*OA*), slow decreasing (*AB*), and rapid decreasing (*BC*), in which the *AB* stage was the main stage of strain rate loading. It can be seen from Fig. 7b that the average strain rates of the specimens increased

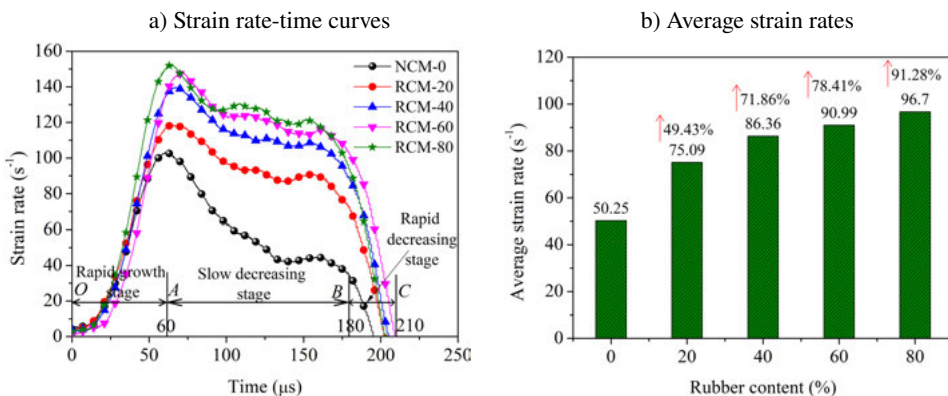


Fig. 7. Strain rate-time curves and average strain rates of specimens under SHPB tests



with the increase of rubber content (the maximum increase is 91.28%), which showed that RCM had better strain rate sensitivity.

### 5. Energy-time curve and energy ratio

The energy-time curves and energy ratio of the specimens under the SHPB impact compression tests are shown in Fig. 8. According to Fig. 8a–8c, the energy-time curves can be divided into three evolution stages: non-energy damage (*OA*), energy damage (*AB*), and energy stability (*BC*). The specific results are as follows:

1. *OA* stage (0 ~ 60 μs): in this stage, the energy was the early energy in dynamic loading, and the reflected energy, transmitted energy, and damage energy were all small, and the smaller early energy does not cause energy damage to the specimen (energy damage is the damage caused by excessive driving energy).
2. *AB* stage (60 ~ 180 μs): in this stage, the energy was the main energy in dynamic loading, and the reflected energy, transmitted energy, and damage energy all increased rapidly. When the energy reaches the maximum energy that the specimen can carry, the specimen will inevitably produce energy damage, and this stage was the main stage of damage to the specimen.

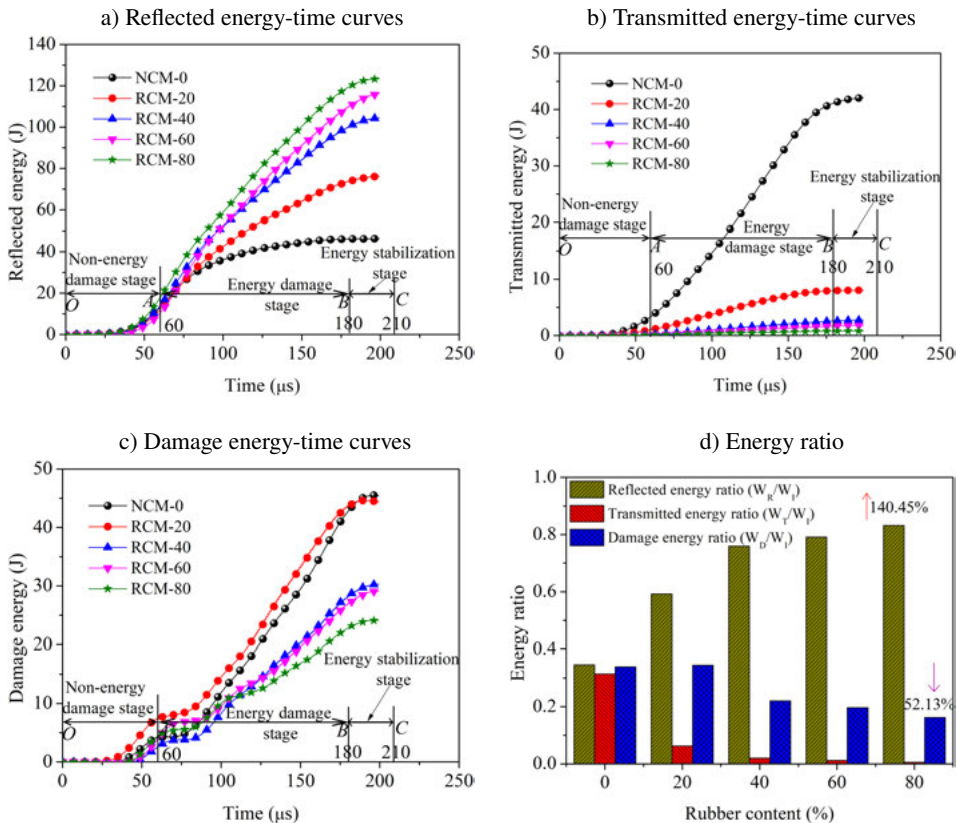


Fig. 8. Energy-time curves and energy ratio of specimens under SHPB tests

3. *BC* stage (180 ~ 210  $\mu$ s): in this stage, the energy was the later energy of dynamic loading, and the reflected energy, transmitted energy, and damage energy tended to be stable, which indicated that the energy damage of the specimen reached the maximum.

As can be seen from Fig. 8d, with the increase of rubber content, the reflected energy ratio and damage energy ratio showed the trend of increasing (the maximum increase is 140.45%) and decreasing (the maximum decrease is 52.13%), respectively. The above results showed that the addition of rubber effectively dissipated the external impact energy and reduced the damage degree of the specimen.

## 6. Dynamic compression damage state

The damage states of the specimens under the SHPB impact compression tests are shown in Fig. 9.

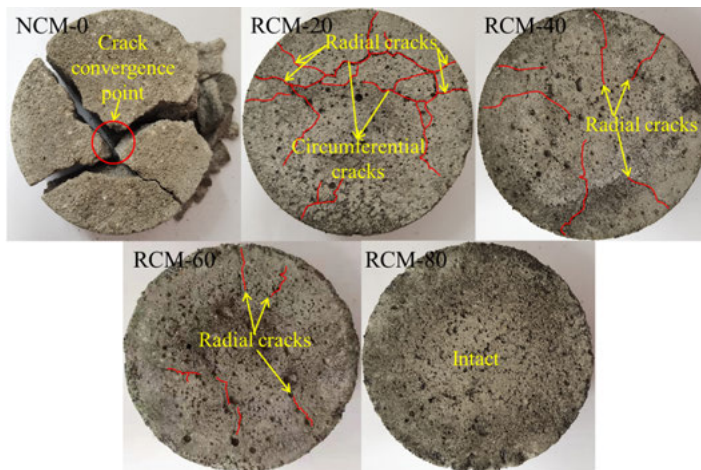


Fig. 9. Damage states of specimens under SHPB tests

As can be seen from Fig. 9, the failure degree of the specimen decreased obviously with the increase of rubber content. The specific manifestations are as follows:

1. The composite compression failure with multiple fracture cracks converging to the central area of the specimen and peeling off at the edge of the specimen mainly occurred in the specimen NCM-0, and the broken fragments had obvious dynamic ejection behavior.
2. The compression damage with edge circumferential-radial compound fine cracks mainly occurred in specimen RCM-20.
3. The compression damage with edge radial fine cracks mainly occurred in the specimens RCM-40 and RCM-60.
- 4) The specimen RCM-80 was basically intact. In conclusion, compared with NCM, RCM showed excellent impact resistance, that was, dynamic impact stability.

### 3.2. High-speed slicing test

#### 1. High-speed slicing state

As can be seen from Fig. 10, under the condition of little difference in slice thickness, the high-speed slicing stability of the specimen was better with the increase of rubber content. In the process of high-speed slicing, NCM was not only constantly ejected the slice fragments, which can not form a complete sheet, but also accompanied by a lot of dust, extremely harsh noise, and obvious sparks (Fig. 10). However, RCM can form a complete sheet, and with the increase of rubber content, dust, noise, and sparks were obviously alleviated (Fig. 10). NCM and RCM showed completely different deformation and fracture characteristics in the high-speed slicing test (Fig. 11).

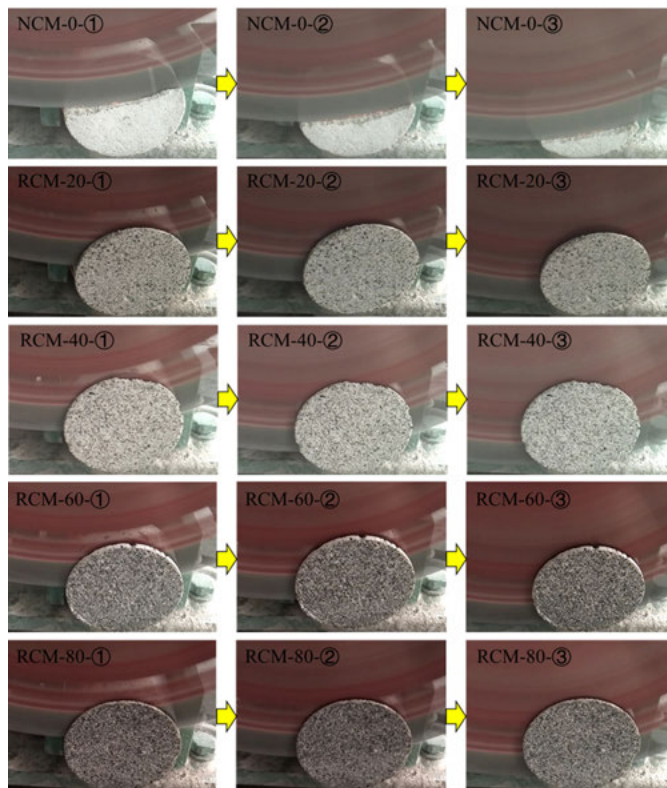


Fig. 10. The high-speed slicing process of specimens with different rubber content

The above fully showed that NCM and RCM showed completely different stability differences in the process of high-speed slicing. The reasons are as follows: 1) When cutting NCM, the high-speed blade and NCM have a “rigid-rigid” confrontation state. The thin slice can not resist the dynamic disturbance of the high-speed blade due to its hard brittleness, which leads to the ejection of the slice fragments (Fig. 11). 2) When cutting RCM, the high-speed blade and RCM form a “rigid-flexible” acceptance state, and

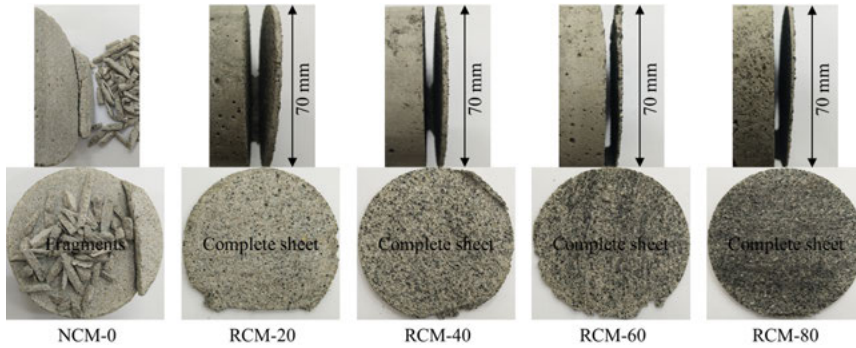


Fig. 11. The high-speed slicing states of specimens with different rubber content

the thinner slice can alleviate the dynamic disturbance of the high-speed blade due to its ductility, thus forming a relatively complete sheet, and the integrity of the slice increased with the increase of rubber content (Fig. 11).

## 2. High speed slicing thickness

The thinnest slice of the parallel specimen with different rubber content was selected as the research object of slice thickness, and the thinnest thickness, maximum thickness, and average thickness of the slice were measured (Fig. 12). In the case of ensuring the integrity of the slice, the thinnest thickness, maximum thickness, and average thickness of the slice decreased with the increase of rubber content, and the relationship between slice thickness and rubber content was a negative linear correlation. The above results fully

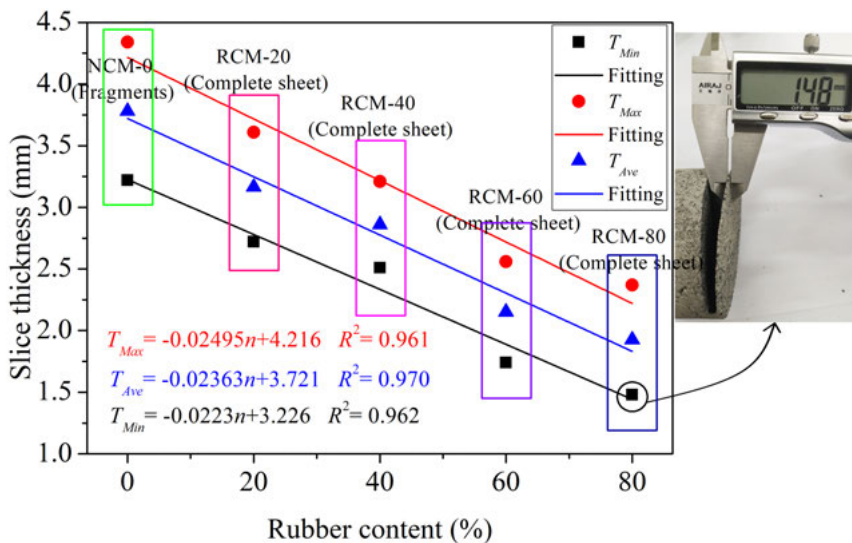


Fig. 12. Thickness of high-speed slices of specimens with different rubber content

showed that rubber particles played a substantial role in effectively improving the stability of high-speed slicing of cementitious composites.

### 3.3. Mesoscopic structure and slicing stability mechanism

The macroscopic failure of the material is essentially represented by the fracture and slip damage of the structure on the mesoscopic scale and microscopic scale [18]. Combined with the high-speed slicing test, the hierarchical structure of the test material is shown in Fig. 13 [18]. For high-speed slicing testing, the mesoscopic structural state of the material can directly reveal the macroscopic slicing stability mechanism of the material.

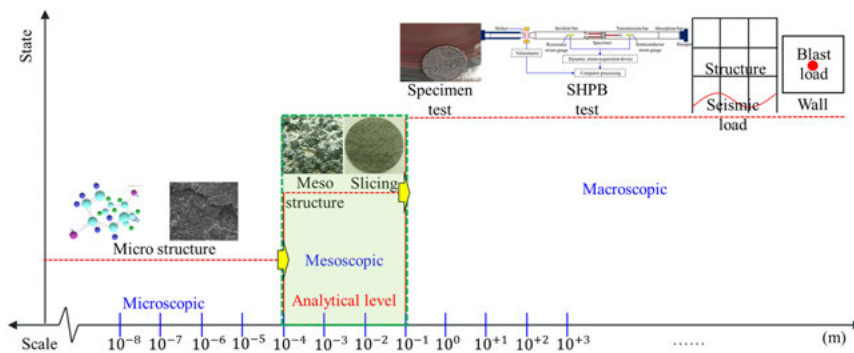


Fig. 13. Hierarchy diagram of testing material

As can be seen from Fig. 14, in the interior of NCM, there was a tight bond between the sand and the hardened cement matrix, and there were only a small number of small pores. However, in the interior of RCM, there was an obvious interfacial transition zone (ITZ) between rubber particles and hardened cement matrix, and there were a large number of pores [19]. From a qualitative point of view, the porosity of the specimen increased with the increase of rubber content, which led to the rougher surfaces of the slices.

According to the SHPB test results and the mesoscopic structure states of specimen slices, the stability mechanism of high-speed slicing can be analyzed from three aspects: stiffness and strength, ductile-plastic deformation, and buffering energy dissipation. The details are as follows:

1. In the aspect of stiffness and strength: From the point of view of structural damage, a large number of pores and rubber particles with low stiffness and low strength in the RCM seriously weakened the stiffness and strength of cement mortar [11], and greatly reduced the cutting resistance of high-speed blade, which provided conditions for effectively reducing the dynamic disturbance under high-speed cutting.
2. In the aspect of ductile-plastic deformation: A large number of pores and rubber particles with high-elastic deformation in the RCM significantly improved the ductile-plastic deformation properties of cement mortar [10]. In particular, a large number of rubber particles with high-elastic deformation made cement mortar had the elastic deformation properties of rubber particles to a certain extent, which greatly reduced the hard-

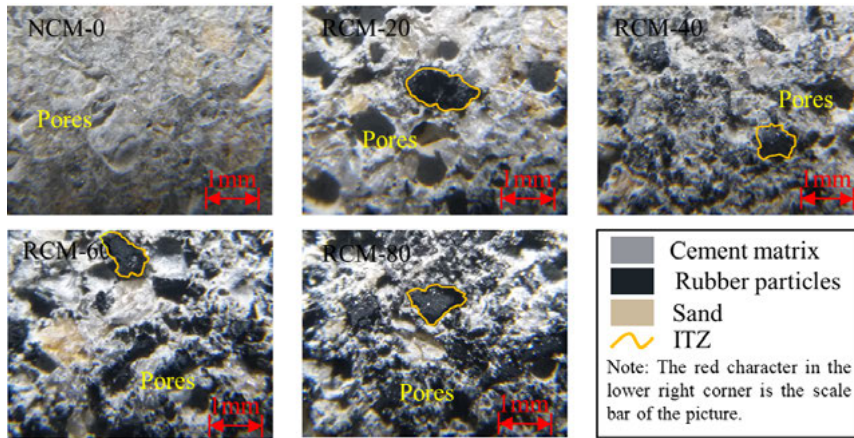


Fig. 14. Mesoscopic structures of specimens with different rubber content

brittleness of cement mortar, which provided conditions for ensuring the deformation stability of the specimen in the process of high-speed slicing.

3. In the aspect of buffering energy dissipation: A large number of pores and rubber particles with high-damping energy dissipation in the RCM effectively improved the buffering energy dissipation performance of cement mortar [19]. In particular, a large number of high-damping energy dissipation rubber particles made cement mortar had the high-damping energy dissipation capacity of rubber particles to a large extent, which provided conditions for the specimen to effectively dissipate dynamic disturbance energy in the process of high-speed slicing.

It should be emphasized that although the strength of RCC with high rubber content is lower, its excellent high deformation, energy dissipation, and crack resistance are worthy of attention. For different engineering applications, there are many methods to solve the low strength problem of RCC. For example, RCC can be used as a “flexible-deformation energy absorption layer” in “rigid-flexible coupling” protective structures [17].

## 4. Conclusion

This work took NCM and RCM as research objects. The SHPB tests with the same impact energy level and the high-speed slicing tests with slice thickness ranging from about 1.4 mm to 4.4 mm were carried out, and the following conclusions were determined:

1. The SHPB test results showed that RCM had excellent impact resistance, mainly in the deformation, energy dissipation, and damage state.
2. The stability of high-speed slicing was better with the increase of rubber content, and the noise and dust were obviously alleviated with the increase of rubber content.
3. In the case of ensuring the integrity of the slice, the minimum thickness of the slice can be better decreased with the increase of the rubber content, and the relationship between slice thickness and rubber content was a linear negative correlation.

4. The porosity inside the cement mortar increased with the increase of rubber content, which led to the rougher surfaces of the slices, resulting in obvious initial structural damage.
5. The SHPB test results and high-speed slicing states fully showed that the flexible RCC had excellent high-ductility-plastic deformation capacity and cushioning energy dissipation capacity, which provides support for the effective application of RCC in disaster prevention and support engineering.

## Acknowledgments

The authors gratefully acknowledge the financial support from the National Natural Science Foundation of China under Grant (52074009) and the Key Research and Development Program Project of Anhui Province (201904a07020081).

## References

- [1] H. Azadmanesh, S.A.H. Hashemi, S.H. Ghasemi, “The effect of styrene-butadiene rubber and ethylene vinyl acetate polymers on the mechanical properties of Engineered Cementitious Composites”, *Composites Communications*, 2021, vol. 24, art. ID 100656, DOI: [10.1016/j.coco.2021.100656](https://doi.org/10.1016/j.coco.2021.100656).
- [2] P. Wang, H. Chen, J. Zhou, Y. Zhou, B. Wang, M. Jiang, F. Jin, H. Fan, “Failure mechanisms of CFRP-wrapped protective concrete arches under static and blast loadings: Experimental research”, *Composite Structures*, 2018, vol. 198, pp. 1–10, DOI: [10.1016/j.compstruct.2018.05.063](https://doi.org/10.1016/j.compstruct.2018.05.063).
- [3] Z. Xiong, Z. Fang, W. Feng, F. Liu, F. Yang, L. Li, “Review of dynamic behaviour of rubberised concrete at material and member levels”, *Journal of Building Engineering*, 2021, vol. 38, DOI: [10.1016/j.job.2021.102237](https://doi.org/10.1016/j.job.2021.102237).
- [4] M. Nehdi, A. Khan, “Flexible crumb tire rubber-filled cement mortars as a protective system for buried infrastructure”, *Journal of ASTM International*, 2005, vol. 2, no. 1, pp. 1–15, DOI: [10.1520/JAI10933](https://doi.org/10.1520/JAI10933).
- [5] I. Khan, K. Shahzada, T. Bibi, A. Ahmed, H. Ullah, “Seismic performance evaluation of crumb rubber concrete frame structure using shake table test”, *Structures*, 2021, vol. 30, pp. 41–49, DOI: [10.1016/j.istruc.2021.01.003](https://doi.org/10.1016/j.istruc.2021.01.003).
- [6] A.O. Atahan, U.K. Sevim, “Testing and comparison of concrete barriers containing shredded waste tire chips”, *Materials Letters*, 2008, vol. 62, no. 21-22, pp. 3754–3757, DOI: [10.1016/j.matlet.2008.04.068](https://doi.org/10.1016/j.matlet.2008.04.068).
- [7] W. Feng, B. Chen, F. Yang, F. Liu, L. Li, L. Jing, H. Li, “Numerical study on blast responses of rubberized concrete slabs using the Karagozian and Case concrete model”, *Journal of Building Engineering*, 2021, vol. 33, DOI: [10.1016/j.job.2020.101610](https://doi.org/10.1016/j.job.2020.101610).
- [8] A. Mohajerani, L. Burnett, J.V. Smith, S. Markovski, G. Rodwell, M.T. Rahman, H. Kurmus, M. Mirzababaei, A. Arulrajah, S. Horpibulsuk, F. Maghool, “Recycling waste rubber tyres in construction materials and associated environmental considerations: A review”, *Resources, Conservation and Recycling*, 2020, vol. 155, DOI: [10.1016/j.resconrec.2020.104679](https://doi.org/10.1016/j.resconrec.2020.104679).
- [9] I. Barišić, M. Zvonarić, I. Netinger Grubeša, S. Šurdonja, “Recycling waste rubber tyres in road construction”, *Archives of Civil Engineering*, 2021, vol. 67, no. 1, pp. 499–512, DOI: [10.24425/ace.2021.136485](https://doi.org/10.24425/ace.2021.136485).
- [10] J. Lv, T. Zhou, Q. Du, K. Li, “Experimental and analytical study on uniaxial compressive fatigue behavior of self-compacting rubber lightweight aggregate concrete”, *Construction and Building Materials*, 2020, vol. 237, DOI: [10.1016/j.conbuildmat.2019.117623](https://doi.org/10.1016/j.conbuildmat.2019.117623).
- [11] T.M. Pham, J. Liu, P. Tran, V.-L. Pang, F. Shi, W. Chen, H. Hao, T.M. Tran, “Dynamic compressive properties of lightweight rubberized geopolymer concrete”, *Construction and Building Materials*, 2020, vol. 265, DOI: [10.1016/j.conbuildmat.2020.120753](https://doi.org/10.1016/j.conbuildmat.2020.120753).

- [12] F. Yang, W. Feng, F. Liu, L. Jing, B. Yuan, D. Chen, “Experimental and numerical study of rubber concrete slabs with steel reinforcement under close-in blast loading”, *Construction and Building Materials*, 2019, vol. 198, pp. 423–436, DOI: [10.1016/j.conbuildmat.2018.11.248](https://doi.org/10.1016/j.conbuildmat.2018.11.248).
- [13] O Youssf, M.A. ElGawady, J.E. Mills, “Experimental investigation of crumb rubber concrete columns under seismic loading”, *Structures*, 2015, vol. 3, pp. 13–27, DOI: [10.1016/j.istruc.2015.02.005](https://doi.org/10.1016/j.istruc.2015.02.005).
- [14] Standards New China. JGJ/T 98-2010: 2010: Specification for mix proportion design of masonry mortar, China Architecture & Building Press, Beijing, China, 2010.
- [15] Standards New China. JGJ/T 70-2009: 2009 Standard for test method of basic properties of construction mortar, China Architecture & Building Press, Beijing, China, 2009.
- [16] R.Z. Yang, Y. Xu, P.Y. Chen, J. Wang, “Experimental study on dynamic mechanics, energy characteristics, and failure mechanism of rubber cement mortar under SHPB splitting test”, *Materials Reports*, 2021, vol. 35, no. 10, pp. 10062–10072, DOI: [10.11896/cldb.20030105](https://doi.org/10.11896/cldb.20030105).
- [17] R.Z. Yang, Y. Xu, P.Y. Chen, “Effect of curing humidity on dynamic compressive failure characteristics and energy dissipation of rubber cement mortar”, *Materials Reports*, 2020, vol. 34, no. 14, pp. 14070–14078, DOI: [10.11896/cldb.19060039](https://doi.org/10.11896/cldb.19060039).
- [18] J. Xu, Z. Yao, G. Yang, Q. Han, “Research on crumb rubber concrete: From a multi-scale review”, *Construction and Building Materials*, 2020, vol. 232, DOI: [10.1016/j.conbuildmat.2019.117282](https://doi.org/10.1016/j.conbuildmat.2019.117282).
- [19] R.Z. Yang, Y. Xu, Q.Q. Zheng, P.Y. Chen, J. Wang, “Fatigue and damage evolution characteristics of rubber cement mortar under graded constant load cyclic compression”, *Journal of Building Materials*, vol. 24, no. 5, pp. 961–969, 2021, DOI: [10.3969/j.issn.1007-9629.2021.05.009](https://doi.org/10.3969/j.issn.1007-9629.2021.05.009).

Received: 20.05.2021, Revised: 24.08.2021